Available online at www.sciencedirect.com
SCIENCE DIRECT®
Experimental Thermal and Fluid Science 29 (2005) 957–970
Experimental Thermal and Fluid Science
www.elsevier.com/locate/etfs

Dynamic dip testing as a method to assess the condensate drainage behavior from the air-side surface of compact heat exchangers

Yongfang Zhong *, Arindom Joardar, Zhongping Gu, Young-Gil Park, Anthony M. Jacobi

Department of Mechanical and Industrial Engineering, University of Illinois, 1206 West Green Street, Urbana, IL 61801, USA

Received 10 June 2004; received in revised form 22 December 2004; accepted 17 January 2005

Abstract

A new method to assess the condensate drainage behavior of the air-side surface of compact heat exchangers—dynamic dip testing—is introduced. The new method is shown to provide highly repeatable data for real-time drainage. Results from experiments with more than 20 flat-tube and round-tube-and-fin heat exchangers are presented, and the data clearly show geometrical effects such as the impact of the tube type on condensate drainage. By comparing the results from dip testing to wind-tunnel experiments for the same heat exchangers, we find dip testing can serve as a powerful tool for assessing the condensate retention behavior. The coils retaining the most and the least condensate in a steady-state wind-tunnel test, likewise held the most and the least in a dip test. However, different amounts of water are retained on the air-side surface during dip tests and wind-tunnel tests. A model based on gravity, surface tension and drag effects is developed to help understand and predict the drainage behavior of heat exchangers. The new model and experimental approach are useful in screening heat exchangers for condensate retention and for assessing off-cycle drainage behavior.
© 2005 Elsevier Inc. All rights reserved.

Keywords: Drainage behavior; Heat exchangers; Dynamic dip testing

1. Introduction

In many applications, air-cooling heat exchangers operate with the heat-transfer surface below the dew point in order to dehumidify the conditioned air. Condensate accumulates on the surface and is retained by surface tension until removed by gravitational or airflow forces. Retained condensate profoundly affects the heat transfer and pressure drop performance and plays an important role in the overall performance of the air-conditioning system. It also has implications on air quality: condensate blown off the heat exchanger surface can directly affect occupant comfort, and water provides a medium for biological activity on air-handling surfaces. Thus, off-cycle condensate drainage is also important, because the warm, moist conditions prevailing after the system shut down are conducive to biological activity. With growing concerns about the quality of conditioned air, designers often strive for heat exchanger designs that provide fast condensate drainage in off-cycle operation. Unfortunately, although there have been numerous studies of the effect of condensate retention on the thermal–hydraulic performance of heat exchangers, very little research in the open literature has addressed the drainage behavior, especially the drainage under off-cycle conditions.

Early studies of liquid retention on heat transfer surfaces were reported in 1948 by Katz and Geist [1], who conducted experiments with pure R-12, *n*-butane, acetone, and water vapor, supplied by a boiler and

* Corresponding author. Tel.: +1 217 244 8830; fax: +1 217 244 6534.
E-mail address: yzhong1@uiuc.edu (Y. Zhong).

0894-1777/$ - see front matter © 2005 Elsevier Inc. All rights reserved.
doi:10.1016/j.expthermflusci.2005.01.006

Nomenclature

A_T	total (air-side heat transfer area (m^2)
C_0	loss coefficient (–)
CV	control volume
CS	control surface
D_h	hydraulic diameter (m)
F	force acting on control volume (N)
F_p	fin pitch (m)
L	vertical length of a heat exchanger (m)
L_p	louver pitch (m)
M	mass of water in control volume (g)
P	pressure (N/m^2)
s	instantaneous drainage distance (m)
t	time (s)
V	volume (m^3)
v	velocity (m/s)
w	fin depth (m)
x	vertical coordinate (m)

Greek letters

α	louver angle (°)
δ	tube pitch (m)
μ	viscosity (N s/m^2)
ρ	density (kg/m^3)
σ	surface tension (N/m)
θ_R	receding contact angle of water on the fin surface

Subscripts

s	surface force
b	body force
fin	fin
g	gravity
max	maximum
pr	pressure force

condensed on six horizontal finned tubes in a vertical column. Katz and Geist developed a model based on the assumption that gravity is the dominant force to drain condensate from the condensing surface. On the basis of that assumption, they calculated the values of the heat coefficient from Nusselt theory and found that deviations between experimental and theoretically calculated coefficients for the top tube were less than 14% for most fluids, with only a 5% discrepancy for acetone. While it is not possible to simply extend their findings to the complex geometries used in contemporary heat exchangers or to situations with binary or multi-component mixtures, their experiments and modeling demonstrate the importance of understanding drainage behavior in order to predict thermal performance.

Karkhu and Borovkov [2], Rifert et al. [3], Honda et al. [4], and Rudy and Webb [5] focused their research on the surface tension force during condensate retention. They proposed that surface tension could be a dominant force in condensate drainage for the integral-fin tube of their studies. Rudy and Webb [5] conducted static measurements of the amount of condensate forming on an integral-finned tube. Their model to predict the amount of the flooded surface during condensation on a horizontal, integral-fin tube agreed with experiments to within ±10% over most of the test range ($10^{-5} < \sigma/\rho < 8(10^{-5})$ N m^2/kg and $0.73 < F_p < 1.3$ mm).

All of the above research was directed toward integral-fin tube heat exchangers, while Osada et al. [6,7] performed heat transfer and condensate visualization studies using single-fin models of flat-tube evaporators. They examined the effects of surface wettability, louver geometry, and heat exchanger inclination. Osada et al. [6,7] concluded that fin geometry, wettability, and the characteristics of the airflow—especially at the exit face of the heat exchanger—were important factors in condensate drainage. They also found that coil inclination greatly influenced the thermal performance of an evaporator.

Recently, McLaughlin and Webb [8] examined fin geometry effects on drainage and retention characteristics using a tabletop apparatus to study a single-fin which was brazed to a plate chilled by circulating "ice-water" through a tube brazed to it. Their scheme allowed optical access to the fin during the formation and subsequent drainage of condensate. McLaughlin [9] also compared the retained water measured in their "dip test" to that measured in a wind tunnel. They weighed a dry coil, dipped it in a bucket of water, removed it from the water and began to weigh the wet coil after 15 s. The heat exchanger was allowed to drain for 120 s in the vertical position, and then a thin piece of aluminum was touched to the bottom of the core to remove water clinging to the lower manifold. They found the mass of remaining water to be within 10% of that measured in a wind tunnel. The remaining condensate (per fin) in their dip test was found to be 3% lower than that in their single-fin tests. It should be noted that all wind-tunnel experiments were conducted with the air frontal velocity of 2.4 m/s, and the dip test was conducted in quiescent surroundings. The findings to be presented in this paper will show the dependence of condensate retention on frontal velocity; we will also demonstrate that the time dependence of drainage can be markedly different for different geometries and wettability conditions. The findings to be presented in this paper will stand in contrast to the earlier work of Webb and McLaughlin.

Although prior research has shown that air-side condensate retention has an important effect on the thermal–hydraulic performance of compact heat exchangers, limited work has been reported on measuring retention and drainage from the air-side surface. One approach to such measurements is to measure the mass of a heat exchanger operating under dehumidification conditions in a wind (see [10]). In this paper, we will describe a new method for assessing condensate drainage from a compact heat exchanger. In the new method, which we will refer to as *dynamic dip testing*, a heat exchanger is submerged in a tank while suspended on a mass balance; the water level in the tank is suddenly reduced and the weight of the heat exchanger is measured as a function of time. This method is simple, inexpensive, and relatively fast. By comparing dynamic-dip-test data to data from wind-tunnel experiments with the same specimens, we will establish the general value of dynamic dip testing as a screening tool. Furthermore, we will present a preliminary model of water drainage in dynamic dip testing; the model provides an estimation of the length of initial water drainage period and other insights into the factors important for water drainage and retention.

2. Methods

2.1. Dynamic dip testing

Two different apparatus were used for dip testing, both are shown schematically in Fig. 1. The first apparatus (Fig. 1a) consisted of a moving water reservoir and simple mounting hardware to suspend and weigh the heat exchanger. The moving reservoir had a volume of 0.068 m^3, and it was positioned using a hydraulic jack to allow a smooth, consistent lowering. Experiments could be conducted with the test specimen tilted from the vertical orientation. For each dynamic dip test, a dry test coil was suspended over the water reservoir and the alignment was confirmed. After the balance was zeroed, the water reservoir was raised to immerse the specimen. The water was agitated to remove air trapped on the air-side heat transfer surfaces, before the reservoir was lowered. Beginning at the instant when the water level reached the bottom of the heat exchanger, mass readings were recorded at 5-s intervals for 90 s and then at 30-s intervals for additional 240 s. Experiments of longer duration were also conducted to help fully characterize the nature of water drainage.

All heat exchangers tested in this apparatus were of the plate-and-fin construction typical to the automotive industry, as shown in Fig. 2. Geometric specifications for the specimens are provided in Table 1, corresponding to the figure. Three basic fin types were used: a conventional louver fin, a conventional offset-strip fin, and a

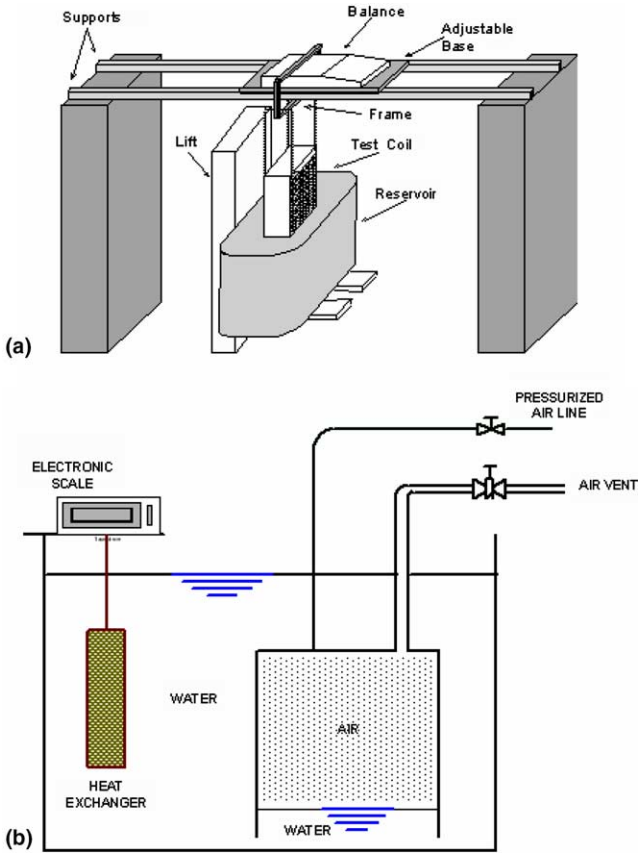

Fig. 1. Schematic of the two dynamic dip testing apparatus: (a) the first, apparatus A, was based on a moving-reservoir design, and (b) the second, apparatus B, was based on water-volume displacement.

combination fin. The combination fin for coil 4 and 5 is shown in Fig. 2b; it consisted of an offset-strip fin between two louver banks. The louvers constituted approximately 90% of the heat transfer area. Coils 3 through 5 were tested both vertically and titled at a 10° angle. An electronic balance (Sartorius, LC12000S) with a reported uncertainty less than 0.1 g was used. The mass data were recorded manually at intervals determined using a stop watch, and the estimated uncertainty in recording time is less than 0.5 s. Through repeated dip-test experiments, standard error propagation techniques were used to find an overall uncertainty of 6% of the reading.

The second apparatus (see Fig. 1b), consisted of a large water reservoir, a smaller submerged air reservoir to control the submersion of coils by displacement of water using compressed air, and a structure to suspend and weigh the heat exchanger. The heat exchanger was suspended from a balance using a fixed acrylic frame and simple mounting hardware. Before an experiment, the balance was turned on and zeroed after the test coil was suspended over the reservoir. At this point, the displacement tank was filled with water, and a final heat exchanger alignment check was performed. In order to

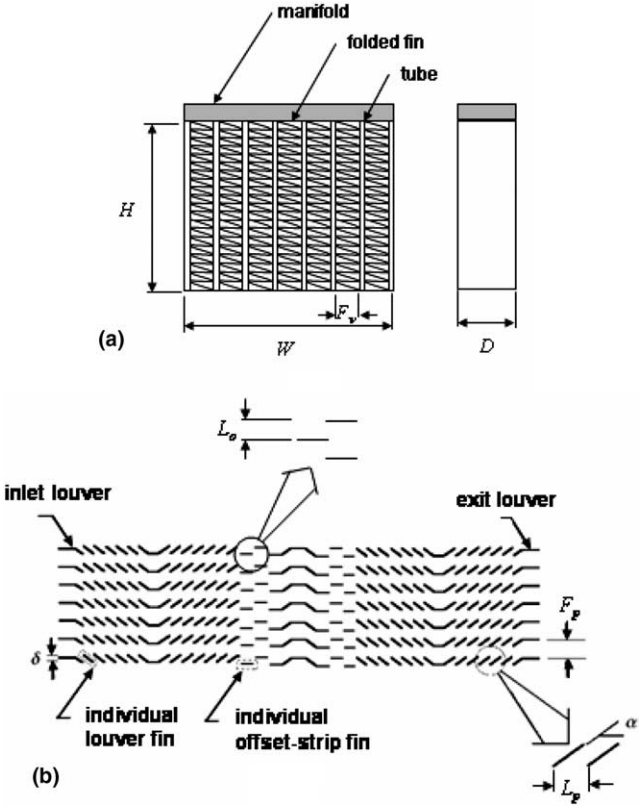

Fig. 2. Schematic of the coils used in apparatus A: (a) an overall view of the heat exchanger geometry, and (b) a detailed representation of a fin array (the combination fin is shown).

initialize a test, the air vent was then closed, and the air supply was used to fill the displacement tank, causing the water level to rise and submerge the test specimen. Once the specimen was submerged, the air supply was closed. The water in the tank was agitated, and a fine brush was used to remove bubbles from the heat exchanger surface. While recording weight data, the air vent was suddenly opened to allow water into the displacement tank. The water level in the main reservoir dropped faster than 0.2 m/s.

The heat exchangers tested in the second apparatus are shown in Fig. 3, with geometric specification provided in Table 2. In Table 2, coils 8 through 11 and coils 15 through 25 are used in automotive radiator systems, and coils 13 and 14 are round-tube heat exchangers typical to residential air-conditioning systems. All the specimens were tested in a vertical orientation, coils 8 through 11 were tested at 5° and 10° tilt angles, and coils 15 through 18 were tested at 10° tilt angles. The estimated uncertainty in the tilt angle was 1°. The same balance was used in all testing. A computer-based data acquisition system with a minimum recording interval of 0.1 s was used for the mass measurements, and the instrument uncertainty is adopted as the mass measurement uncertainty for these computer-timed data.

The simple procedures for the dynamic dip test with these two apparatus are essentially the same: submerge the test sample in the water, and measure the real-time water retention on the heat exchangers during water drainage. The second apparatus was developed as a refinement to the first, given the apparent success of the method. However, now we wish to report data from both apparatus, with all data from the second, refined apparatus, except for data from coils 1 to 7, which were obtained with the first apparatus.

2.2. Wind-tunnel testing

Complementary wind-tunnel experiments were conducted using the closed-loop wind tunnel shown schematically in Fig. 4. The wind tunnel consisted of an axial blower with a frequency-controlled drive, electrical

Table 1
Geometrical description of the coils tested in apparatus A (all dimensions in mm)

Coil	External dimensions ($H \times W \times D$)	Fin type	Louver pitch L_p	Louver angle α (°)	Louver width L_w
1	$213.0 \times 219.0 \times 92.0$	Louver	5.08	N/A	6.35
2	$209.6 \times 203.2 \times 76.2$	Louver	1.59	N/A	6.35
3	$215.9 \times 228.6 \times 58.0$	Louver	1.20	30	6.35
4	$215.9 \times 228.6 \times 58.0$	Combo	1.00	36	6.35
5	$215.9 \times 228.6 \times 58.0$	Combo	1.00	42	6.35
6	$242.9 \times 292.1 \times 58.0$	Offset	1.19	0	8.51
7	$190.5 \times 247.7 \times 76.2$	Offset	1.27	0	6.35

Coil	Fin width L_f	Fin thickness δ	Fin pitch F_p	Offset height L_o	Contact angle (°)	
					Advancing	Receding
1	9.14	0.13	2.12	–	64	35
2	9.53	0.13	2.12	–	60	30
3	8.00	0.10	1.81	–	68	44
4	8.00	0.10	1.81	–	68	44
5	8.00	0.10	1.81	–	68	44
6	9.73	0.09	1.81	0.64	46	30
7	9.40	0.10	1.69	0.85	48	31

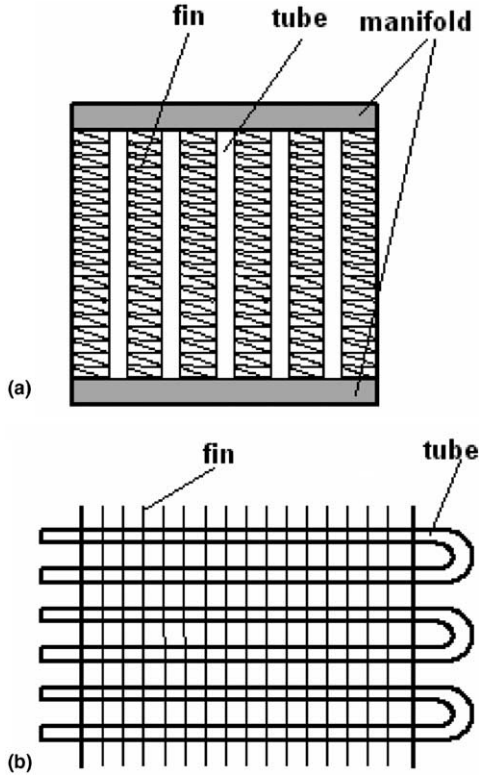

Fig. 3. Schematic of the coils used in apparatus B: (a) the flat-tube heat exchanger, and (b) the round-tube heat exchanger.

resistance heaters, a steam injection system with a PID controller, a large thermal mixing chamber, a flow conditioning section of screen and honeycomb, and a flow contraction to the test section. During an experiment, the test heat exchanger was supplied with a single-phase

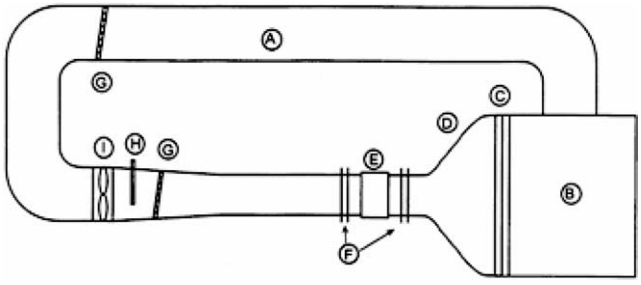

Fig. 4. Schematic of the wind tunnel used for real-time and steady state condensate measurement: (A) return duct; (B) thermal mixing chamber; (C) Screens and honeycomb flow conditioning; (D) 9:1 flow contraction; (E) test heat exchanger; (F) measurement locations; (G) resistance heaters; (H) steam injection tube; (I) axial blower.

ethylene-glycol coolant flow from a chiller system (not shown in the figure). The wind-tunnel apparatus provided an air flow from about 0.5 to 5 m/s, with controlled velocity, temperature, and humidity. Measurement stations included a six-junction thermocouple grid upstream of the test section, and a twelve-junction grid downstream of the test section. The approaching flow was isothermal to within 0.8 °C in the worst case (at the lowest air velocity), and the velocity deviation from the mean was always less than 11%, with a turbulence intensity less than 2.5%. The same balance for the dip tests was used in the wind tunnel and the air velocity was measured using a constant-temperature thermal anemometer, with an uncertainty of less than 2% of the reading. This apparatus is described in more detail elsewhere [11,12]; however, because our purpose now is only to report mass data—not thermal–hydraulic

Table 2
Geometrical description of the coils tested in apparatus B (all dimensions in mm)

Coil	External dimensions ($H \times W \times D$)	Louver angle (°) α	Louver pitch	Tube type	Tube dimensions				Fin type	Fin dimensions	
					Number of tubes	Width or diameter	Depth	Wall thickness		Thickness δ	Fin pitch F_p
8	406.4 × 381.0 × 15.9	27	1.40	Flat	38	1.84	13.54	0.41	Louver	0.18	1.11
9	406.4 × 381.0 × 27.9	27	1.40	Flat	38	1.88	25.40	0.41	Louver	0.18	2.00
10	406.4 × 381.0 × 15.9	27	1.40	Flat	38	1.84	13.54	0.41	Louver	0.18	2.00
11	406.4 × 381.0 × 27.9	27	1.40	Flat	38	1.88	25.40	0.41	Louver	0.18	1.11
12	228.6 × 266.7 × 73.0	NA	NA	Flat	21	3.43	73.02	NA	Louver	0.09	2.00
13	203.2 × 381.0 × 37.7	NA	NA	Round	16	10.20	NA	0.10	Louver	0.10	1.43
14	203.2 × 254.0 × 44.4	NA	NA	Round	16	9.52	NA	1.08	Plain	0.10	1.67
15	240.0 × 254.0 × 58.0	43	1.0	Flat	23	1.88	58	NA	Louver	0.09	1.59
16	215.0 × 241.0 × 89.0	30	2.23	Flat	21	3.05	89	NA	Louver	0.09	2.12
17	220.0 × 264.0 × 75.0	NA	NA	Flat	22	NA	75	NA	Louver	NA	1.81
18	229.0 × 259.0 × 73.0	NA	NA	Flat	20	NA	73	NA	Louver	NA	1.95
19	238.0 × 232.0 × 58.0	35	1.28	Flat	21	1.88	58	NA	Louver	0.09	1.59
20	238.0 × 232.0 × 58.0	NA	NA	Flat	21	1.88	58	NA	Louver	0.09	1.69
21	238.0 × 232.0 × 58.0	NA	NA	Flat	21	1.88	58	NA	Louver	0.09	1.81
22	238.0 × 232.0 × 58.0	NA	NA	Flat	21	1.88	58	NA	Louver	0.09	1.59
23	213.0 × 230.0 × 90.0	NA	NA	Flat	19	3.05	90	NA	Louver	0.09	2.12
24	205.0 × 215.0 × 80.0	NA	NA	Flat	17	2.79	80	NA	Louver	0.09	2.31
25	217.0 × 205.0 × 90.0	30	1.50	Flat	18	NA	90	NA	Louver	0.09	2.12

performance—only an overview of these complementary experiments has been provided in this paper.

3. Modeling

A drainage model is developed using a mechanistic approach with a static force balance as a basis. Heat exchanger types (round tube or flat tube) and fin geometries are considered in developing this model. For the round-tube model, the control volume is taken as the space between two adjacent fins, with the tubes neglected. For the flat-tube heat exchanger, the control volume is slightly more complex, enclosing the space between two neighboring tubes but not the fins, as shown in Fig. 5.

The drainage paths for both the round- and the flat-tube geometries are approximated as a vertical flow. At time zero, the control volume is full of water (submerged condition); at this point the heat exchanger is holding the maximum amount of water, $M_{\max}$. Once the drainage process begins, $0 < M(t) < M_{\max}$, and $0 < s(t) < L$, where L is the total length of drainage path, i.e., the height of the heat exchanger.

We adopt the following assumptions for a momentum balance on the control volume: (1) the control volume is fixed; (2) the density of water is much larger than the density of air; (3) the velocity is uniform over the control surface; (4) the velocity is uniform in the control volume; (5) all thermophysical properties are constant. The model is also tacitly restricted to vertically oriented heat exchangers, because when a heat exchanger is tilted, the drainage path is altered.

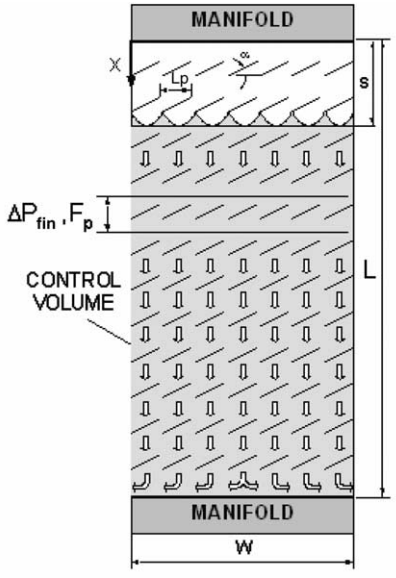

Fig. 5. The control volume, coordinate system, and water drainage path for flat-tube heat exchanger in vertical direction.

For the flat-tube case, a pressure is exerted on the bottom of the control volume, because the flow encounters the manifold and is turned 90° and there is no x-momentum flux crossing the control surface. The magnitude of this pressure is determined by considering an infinitesimal control volume above the manifold and equating the x-momentum flux to the pressure.

The conservation of x-momentum may then be written as

$$\sum F_{sx} + \sum F_{bx} = \frac{d}{dt} + \int\int\int_{CV} v_x \rho \, dV + \int\int_{CS} v_x \rho v_x \, dA \tag{1}$$

with F_{sx} representing surface forces, and F_{bx} body forces in the x-direction, respectively.

With the definition of control volume and the assumptions, the instantaneous distance of drainage is defined as s, and the velocity in x-direction is

$$v_x = \frac{ds}{dt}. \tag{2}$$

Surface forces include viscous forces on the flowing water, surface tension, and pressure. Thus, accounting for their x-direction, we may write

$$\sum F_{sx} = -F_\mu - F_\sigma - F_{pr}. \tag{3}$$

Gravity is assumed to be the only body force, and thus

$$\sum F_{bx} = F_g. \tag{4}$$

For the round-tube geometry, with the stated assumptions, the right-hand-side (RHS) of Eq. (1) can be written as

$$\text{RHS} = \rho F_p w \left\{ (L-s)\frac{d^2 s}{dt^2} - \left(\frac{ds}{dt}\right)^2 \right\} + \rho F_p w \left(\frac{ds}{dt}\right)^2. \tag{5}$$

The viscous, surface tension, and gravitational forces are, respectively (Note there is no pressure force for the round-tube case, because there is no manifold):

$$F_\mu \approx A_T \left(\frac{L-s}{L}\right) \frac{6\mu}{F_p} \frac{ds}{dt}, \tag{6}$$

$$F_\sigma \approx 4 w \sigma \cos\theta \tag{7}$$

and

$$F_g \approx \rho g F_p w (L-s). \tag{8}$$

For the flat-tube geometry, with the assumptions stated, the RHS of Eq. (1) is

$$\text{RHS} \approx \rho \delta w \left\{ (L-s)\frac{d^2 s}{dt^2} - \left(\frac{ds}{dt}\right)^2 \right\}. \tag{9}$$

The viscous force in the flat-tube geometry with louver fins is approximated by the pressure-drop effect by parallel blade dampers as illustrated in Fig. 5. Although this model is for a laminar flow of water, as a first approximation, we used the tabulated loss-coefficient data for air-flow dampers in the literature is used [13]. The pressure drop by a single fin can be written as

$$\Delta P_{\text{fin}} = \frac{C_0}{2}\rho\left(\frac{\mathrm{d}s}{\mathrm{d}t}\right)^2, \tag{10}$$

where C_0 is the loss coefficient. Then, the viscous force is

$$F_\mu \approx \Delta P_{\text{fin}}\left(\frac{L-s}{F_{\text{p}}}\right)w\delta. \tag{11}$$

The surface tension force is calculated for thin sheets of water attached to the bottom of louvers (see Fig. 5),

$$F_\sigma \approx \frac{2w}{L_{\text{p}}}\sigma\delta. \tag{12}$$

The pressure and gravitational forces are

$$F_{\text{pr}} \approx \rho w\delta\left(\frac{\mathrm{d}s}{\mathrm{d}t}\right)^2 \tag{13}$$

and

$$F_{\text{g}} \approx \rho g\delta w(L-s). \tag{14}$$

In the development of the flat-tube model, each louver is approximated to span the distance between neighboring tubes. The loss coefficient, C_0, is given as a function of louver pitch (L_{p}), louver angle (α), and other fin dimensions [13].

From Eqs. (1)–(14), it is apparent that the round-tube and the flat-tube drainage models consist of nonlinear, second-order, ordinary differential equations for the drainage distance $s(t)$. In order to solve these equations, we impose $s = 0$, and $\mathrm{d}s/\mathrm{d}t = 0$ at $t = 0$. The differential equations are then integrated numerically, using a commercial package to perform a fifth-order Runge–Kutta–Verner integration, with a relative residual less than 10^{-6}. The solution for $s(t)$ can be rearranged to give the mass of water remaining in the drainage path $M(t)$.

4. Results and discussion

The results from dynamic dip testing will be presented first, followed by the results from real-time and steady-state condensate retention in the wind tunnel. We report experimental and modeling results for both vertical and tilted heat exchangers.

Both apparatus for dynamic dip testing exhibit excellent repeatability, as demonstrated by the example results from several experiments with one heat exchanger in Fig. 6. Dynamic dip test results in the form of mass per unit air-side heat transfer area as a function of time are shown in Fig. 7 for heat exchangers in a vertical orientation. The general behavior of the data shows a monotonic decrease in the retained water. It is interesting to note two distinct drainage patterns in the data (cf. Fig. 7a and b). In Fig. 7a, 80% of the water that will ultimately leave the coil drains during the first 20 s. We refer to a drainage behavior in which the mass change is very fast initially, and for which an asymptotic retention is attained after a very short time (on the order of 20 s) as a *steady-retention pattern*; whereas, in Fig. 7b it is clear that drainage continues well after the first 20 s, and we call that second behavior a *continuous-drainage pattern*. In order to test the generality of these observed drainage patterns, we selected four flat-tube, louvered-fin heat exchangers (coils 15–18) with similar geometries to subject to testing in Apparatus B. The main difference between these four

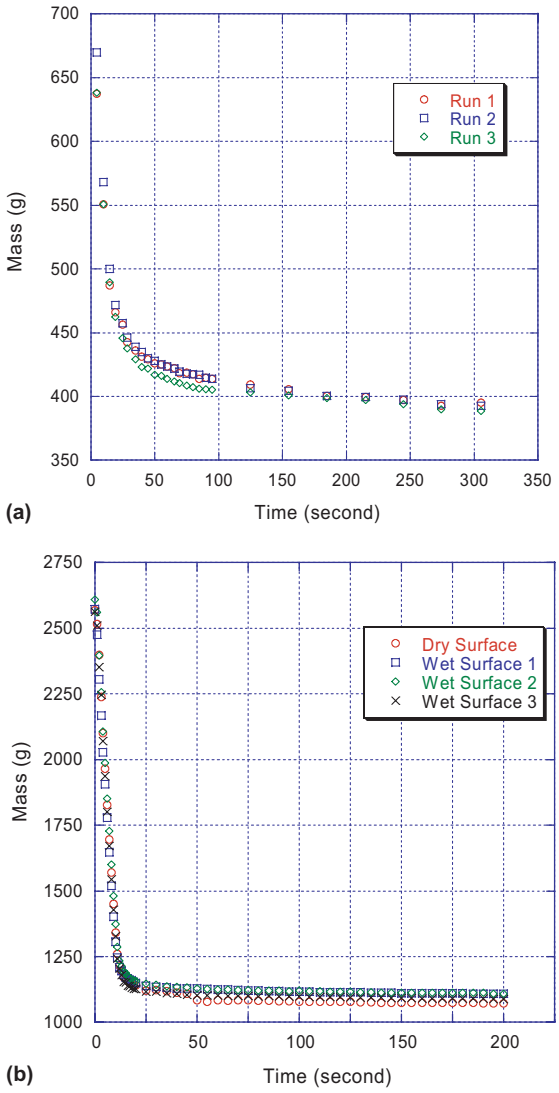

Fig. 6. Data from repeated experiments, illustrating the reproducibility of the new methods: (a) coil 3 in apparatus A, and (b) coil 11 in apparatus B. These results are typical to those using other coils.

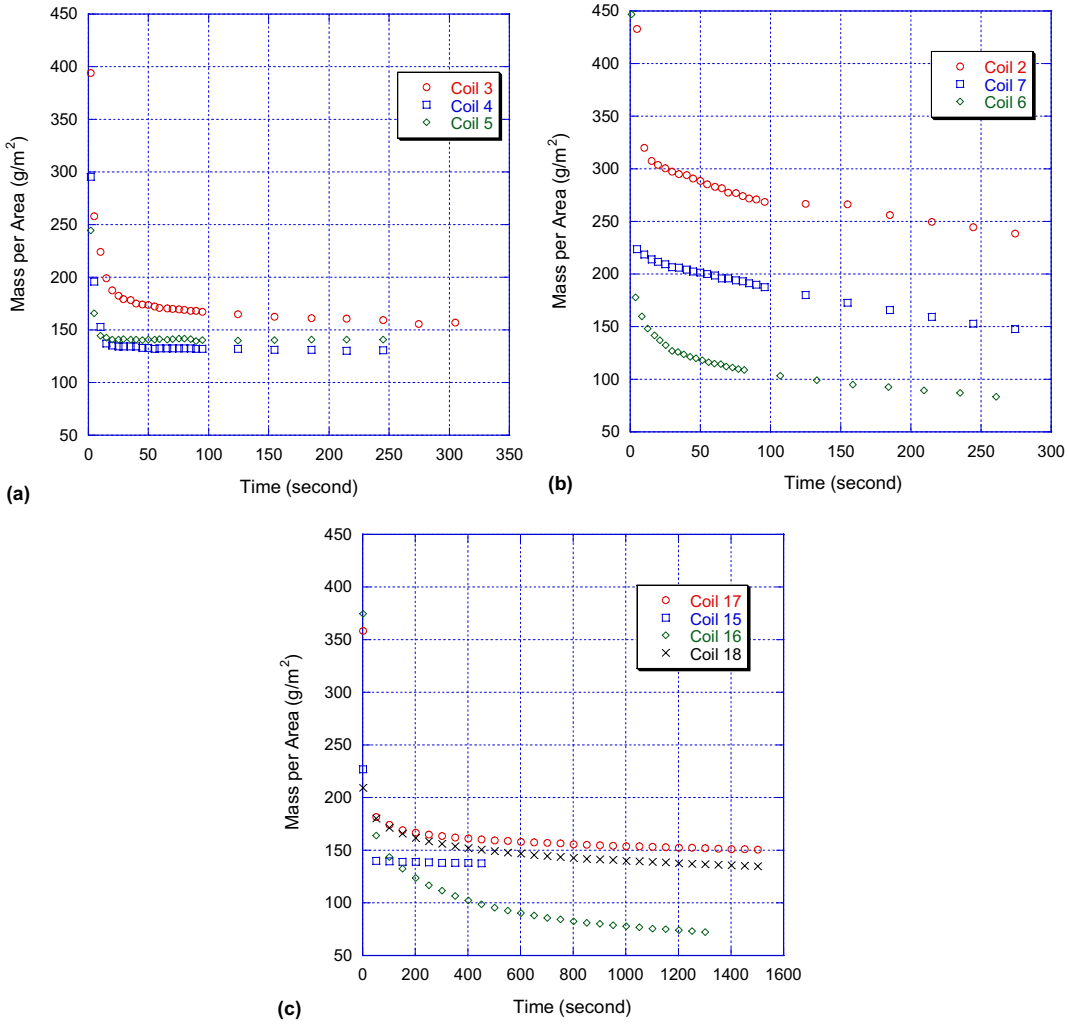

Fig. 7. The mass of water retained on the coil per unit air-side heat transfer area is shown as a function of time. In (a) the data show a so-called *steady* retention pattern; whereas in (b) a *continuous* drainage pattern is manifest; other data are shown in (c) where both drainage patterns are evident.

coils rests in their fin density—coil 15 had the highest fin density and only one manifold at the top. Coil 16 has a lowest fin density and two manifolds, one at the top and one at the bottom; while the fin densities of coil 17 and 18 are between those of 15 and 16. From Fig. 7c more than 80% of the water that will eventually leave the coils drains during the first 50 s in coil 15 and 17; On the other hand, coil 16 and 18 continue to drain even after the initial 50 s at a good rate. Coil 15 and 17 show a steady-retention pattern while coil 16 and 18 show a continuous-drainage pattern. Another interesting feature is that coil 15 has a sharp transition to a steady-state after the initial free-fall type drainage, in contrast to the slow transition for coil 16. We suspect that gravitational and viscous forces are more important in the drainage of coil 16 than that in coil 15. These differences in drainage patterns may be due to geometrical differences between the coils, but it is difficult to ascertain the exact causes of their patterns.

An important trend evident in Fig. 7 is that the louver fin coils hold more water per unit area than the combination coils do, and combination coils generally hold more than offset-strip fin coils do at a given time. This finding is evident in Fig. 7, where the louvered fins (coils 2 and 3) hold the most water, retaining 160 to more than 220 g/m^2 after about 5 min. In contrast, the offset strip fins retain 100–150 g/m^2, and the combination fins retain 150 g/m^2 after this drainage period. These dynamic dip test data also show the drainage behavior over the first 15 s is very important and suggest static dip testing may be inadequate to fully understand off-cycle drainage but dynamic dip test can provide information on the condensate drainage patterns and insight on fin geometry effects.

Experimental results indicate that water drains more rapidly from a vertical round-tube coil than from a vertical flat-tube one in Fig. 8 in the form of the mass ratio of real-time water retention to possible maximum water

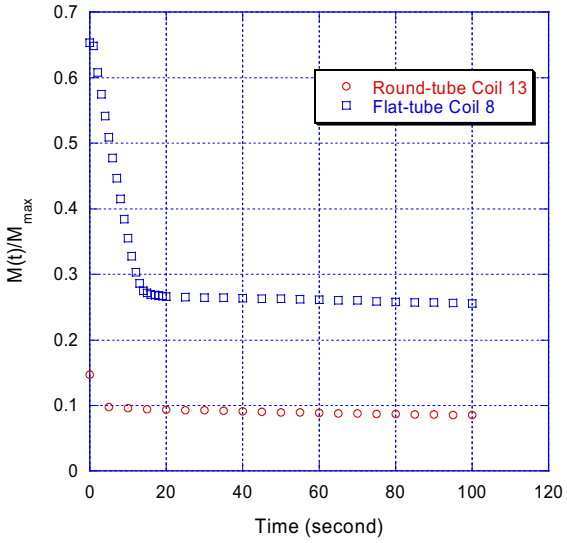

Fig. 8. Experiments to explore drainage patterns for flat- and round-tube heat exchangers, showing water drains more rapidly from a vertical round-tube coil than that from a vertical flat-tube coil.

retention as a function of time. The round-tube coils of this study shed roughly 80% of the water that will drain in a 200-s experiment within 1 s. In contrast, it takes about 10 s for the flat-tube heat exchangers to shed that percentage of the total drainage. These results are summarized in Table 3.

The new drainage model predicts similar trends, with very rapid drainage from a round-tube coil and slower drainage from a flat-tube heat exchanger, as shown in Fig. 9. It should be noted that the model predicts near total drainage from the coil; i.e., $M(\infty) \approx 0$. The model is based on a tacit assumption that drainage is continuous and each louver is span the whole distance between the tubes. However, some water is actually retained on the surface as small droplets, or retained between the neighboring fins near the tube, etc., due to the break-up of the draining film. The experimental data reflect this behavior (Figs. 8 and 9).

A powerful feature of the modeling approach rests in the ability to explore the relevant forces affecting drainage behavior. In Fig. 10, drainage forces are compared between the round-tube and the flat-tube heat exchangers, respectively. For the round-tube geometry, as time passes the velocity increases and a viscous force develops. The magnitude of viscous force grows to nearly

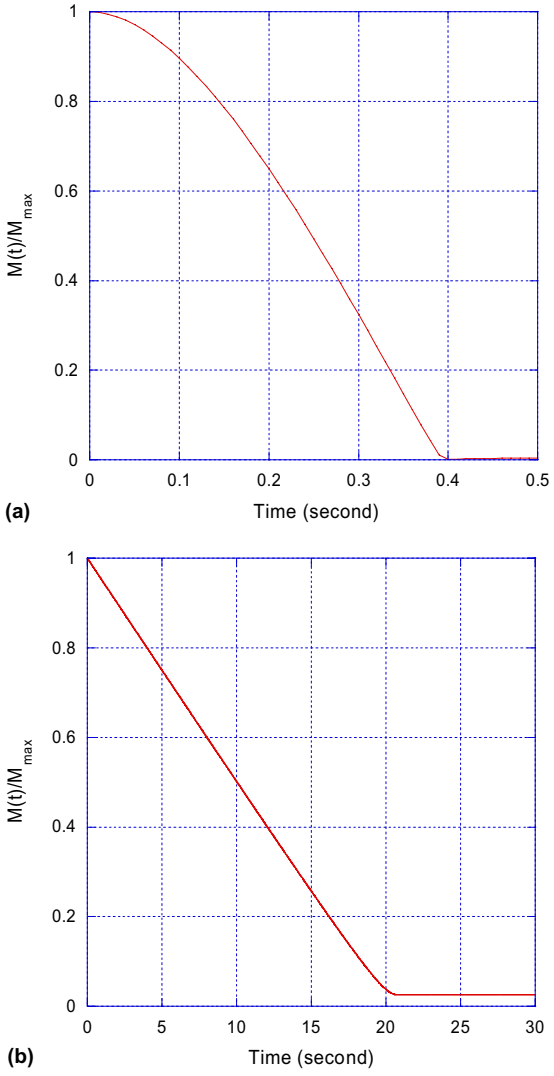

Fig. 9. Modeled drainage behavior for two types of heat exchangers: (a) prediction for round-tube coil 13, and (b) prediction for flat-tube coil 8.

80% of the gravitational force in time, and the flow continues to accelerate throughout the drainage process. The situation is quite different for the flat-tube geometry. The viscous force is more dominant in the flat-tube geometry, because drainage in the flat-tube geometry is through a very small inter-louver gap, causing a bigger viscous force than a more open drainage path of the round-tube geometry will. Initially, with zero drainage

Table 3
A comparison of overall drainage behavior for round-tube and flat-tube coils

Flat-tube coil	$M(10)/M(200)$ (%)	$M(20)/M(200)$ (%)	$M(30)/M(200)$ (%)	Round-tube coil	$M(1)/M(200)$ (%)
8	72.4	93.8	94.0	13	82.6
9	77.6	88.3	95.0		
10	82.0	89.6	95.5	14	87.0
11	82.0	95.4	96.6		
12	76.0	91.3	95.7		

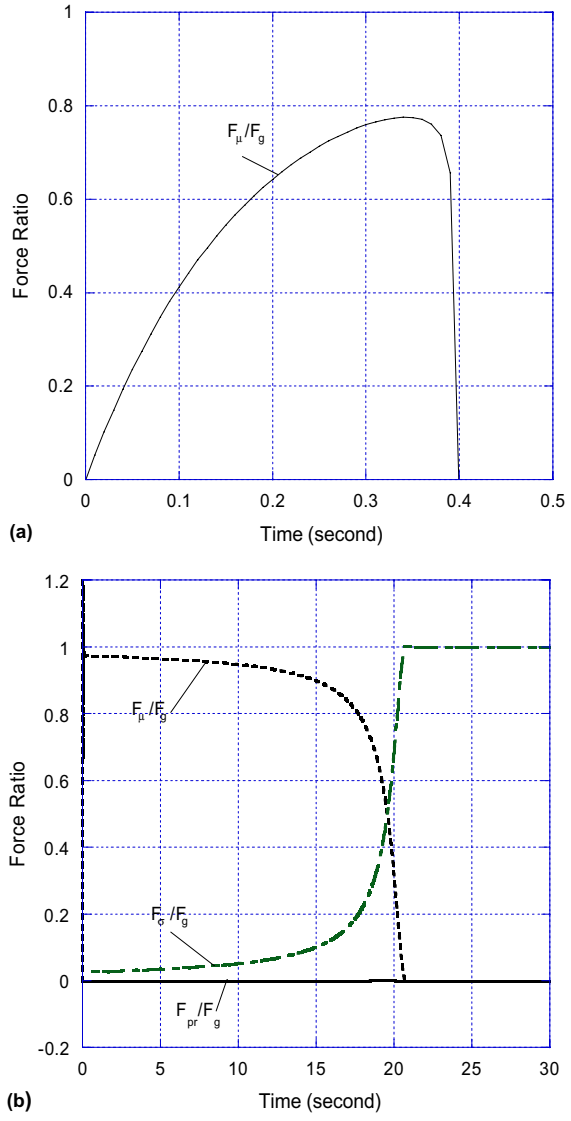

Fig. 10. The relative magnitudes of forces relevant to water drainage as predicted by modeling: (a) for a round-tube coil, and (b) for a flat-tube coil.

velocity the viscous force is zero. However, as the drainage begins, the viscous force quickly rises to fully counter the gravitational force and the flow remains at a nearly constant velocity until the end of the drainage period. The pressure force is much smaller than the viscous or gravitational forces, and it is coupled to the velocity. Although the surface tension force in both round- and flat-tube models are substantially underestimated as a result of the assumptions, there still appears some effect in the results, especially in the flat-tube model (Fig. 9b). The steady-state retention in the model appears due to the retention at the bottom of the heat exchanger, which is real in experiments.

Another interesting facet of the experimental data is how drainage behavior appears to be related to the heat exchanger hydraulic diameter. Coils with similar air-side hydraulic diameters (coils 8 and 11 have the same air-side hydraulic diameter; the same for coils 9 and 10) have similar drainage patterns. The dynamic-dip-test data for two flat-tube heat exchangers, one with twice the hydraulic diameter of the other, are shown in Fig. 11. The coil with a larger air-side hydraulic diameter drains more rapidly near the start of the experiment, and it continues to drain for a longer duration, reaching about 90% of the maximum drainage in comparison to the smaller-hydraulic-diameter specimen, which reaches about 70% of the maximum drainage. For these heat exchangers, the differences in their hydraulic diameters are only by the differences in their fin pitches. Therefore, when the fin density is nearly doubled, the retention after initial drainage is nearly tripled. This behavior indicates that the forms of retention are more that just "louver-bridging", perhaps, "fin-bridging".

The interesting behavior, as shown in Fig. 11, at $10 < t < 30$ for the coil with a large hydraulic diameter might be caused by a change in drainage mechanism. The model prediction in Fig. 11 also shows a faster initial drainage rate with an increase in the hydraulic diameter. In Fig. 11, the durations of drainage predicted by the model show good agreement with the "initial" drainage periods from experiments. The intermediate drainage period between 10 s and 30 s for the sample with a larger hydraulic diameter is not captured by the model. The previous experimental data and the success of the model strongly suggest that the early drainage in the process is through the louver gaps. For a large hydraulic diameter (a large fin pitch), water may pass through the inter-fin space instead—perhaps a thin film, droplets, and a liquid-bridge form. None of these

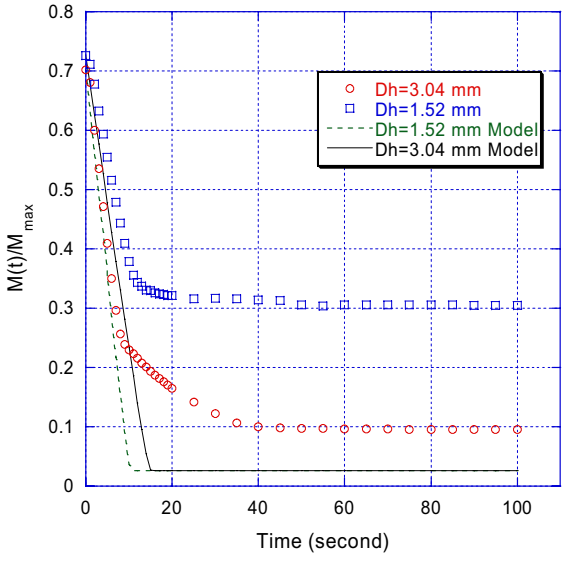

Fig. 11. Drainage patterns for flat-tube coils with different air-side hydraulic diameters, along with a comparison to the model prediction (with initial conditions adjusted per the discussion in the text).

features are captured by the simple model presented in this paper, and further research is required if this behavior is important.

The effects of fin density and fin geometry on drainage were investigated using coils 19–22 which were very similar in their overall size and construction. Coil 19 was very similar to coil 15, with 16 fins per inch and a triangular fin shape when viewed from the air-flow direction. The fin shapes for coils 20–22 were rectangular, with a fin density of 15, 14 and 16 fins per inch, respectively. The dip test results were presented in Fig. 12. As expected, for similar coils an increase in fin density results in increased retention. Although the differences decreased over 1500 s, the trend remained unchanged. On the other hand, the impact of fin geometry was dramatic. Coil 19 with triangular fins (viewed from the air flow direction) held 52.2% more water than its rectangular counterpart, coil 22. The results clearly demonstrate the importance of surface tension effects on drainage behavior and retention. Visual inspection of coil 19 during experiments revealed accumulation of water between fin surfaces in the vicinity of the fin base. Apparently water was drawn up to the fin base and held there by capillarity forces. For the rectangular shape, much greater fin density is necessary for capillarity effects to become important.

The dip testing data for coils 25–27, which have similar geometries but coil 25 with only one manifold at its top and coil 26, 27 with two manifolds, is presented in Fig. 13. The results suggest that in general coils with two manifolds are inherently better drainers than single header heat exchangers. The exact reasons for such wide difference in their performance are difficult to establish in the absence of louver geometrical data. However, during water drainage the heat exchanger without a manifold at the bottom was observed to suffer from the disadvantage of having a closed bottom for structural integrity. It intuitively indicates that a relatively smoothly open bottom with some free passage for the water will facilitate condensate drainage.

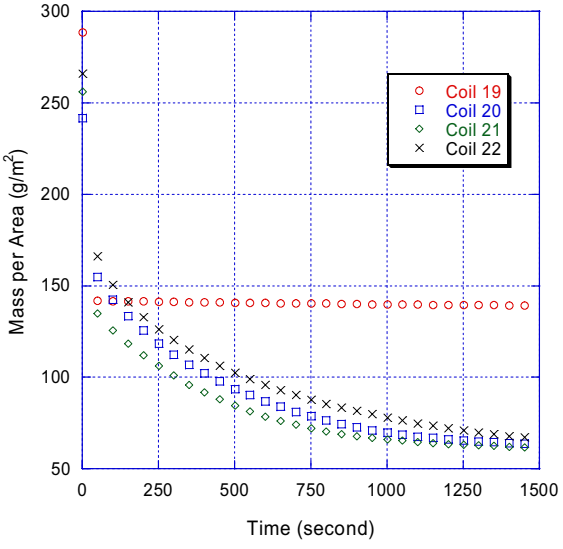

Fig. 12. Data to show the effects of fin density and fin geometry on drainage.

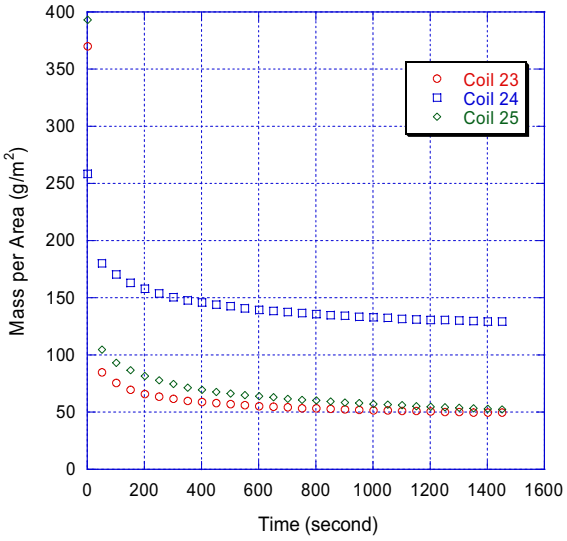

Fig. 13. The effect of manifolds of the coils on drainage.

All the above results are from dip testing in a vertical direction, while the effect of coil inclination on drainage behavior is present in Fig. 14 and Table 4. Fig. 14 demonstrates that tilting the coil does not profoundly affect the nature of the drainage patterns and the drainage behavior of these heat exchangers is affected very little by orientation. It is important to note that the tilt angle of 10° is in the flow direction (i.e., the top of the coil is tilted downstream). This tilt angle promotes condensate flow toward the back of the coil and assists in drainage. The small influence of the tilt angle is probably due to a small impact of tilt on the drainage path. As assumed in the model, drainage is perhaps through the inter-louver gap for all of these tilt angles. It is expected that at some high tilt angles the drainage path will be altered. This result offers indirect support for the model, because the data indicate inter-louver drainage as important, and the model is based on such an assumption.

The amount of water retention at a given time is less for all the tested coils when they are tilted, but the exact reduced amount varies from coil to coil. The data of Table 4 show that an inclination of 10° can reduce the amount of water by roughly 10–25%. When the fin pitch of the coil becomes large, the reduction of water retention caused by inclination may become significant. For example, by comparing Fig. 14c to Fig. 7c, at the end of 1000 s the reduction achieved by 10° tilting was 55.6% for coil 16 which has a larger fin pitch than coil 15, 17 and 18, but only 25%, 11.7% and 23.3% for coils 15, 17 and 18, respectively. The dramatic improvement

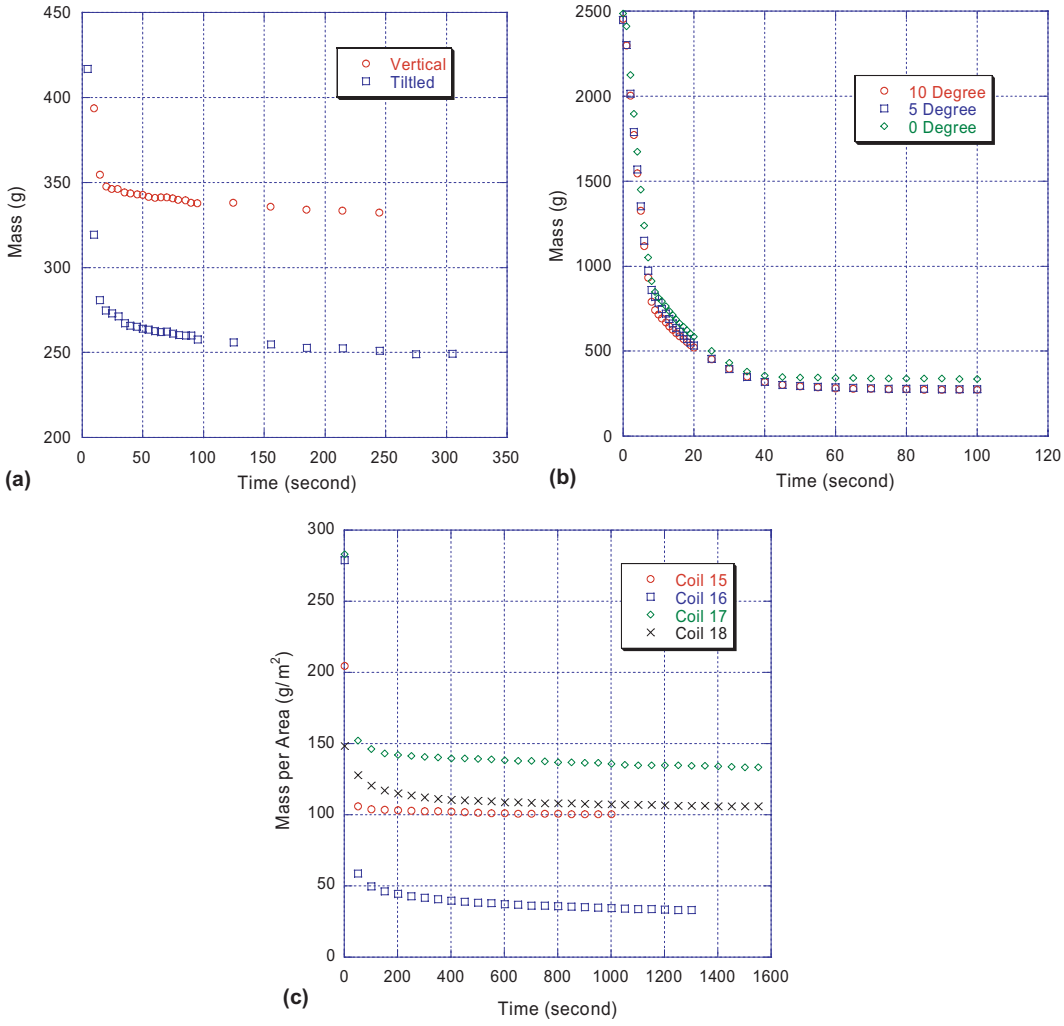

Fig. 14. Dynamic dip experiments to explore the effect of coil inclination on the drainage patterns for flat-tube heat exchangers: (a) coil 4, vertical and at a 10° inclination; (b) coil 11, vertical and at 5° and 10° inclinations; (c) coils 15–18 at 10° inclination.

Table 4
A comparison of retention under the titled and vertical conditions

Coil	Orientation	Mass retained at 20 s	Change (%)	Mass retained at 60 s	Change (%)	Mass retained at 180 s	Change (%)
10	Vertical	414	24	390	25	374	27
	Tilted	325		304		284	
11	Vertical	348	23	342	26	335	27
	Tilted	276		263		254	
12	Vertical	365	12	364	15	362	17
	Tilted	323		312		304	

for coil 16 could be understood in the light of the fact that it is far less compact compared to other coils, hence the resistance to drainage due to surface tension effects is less or probably other drainage paths were developed between its fins.

Representative real-time condensate retention data for coil 4 are given in Fig. 16 for two face velocities and almost the same humidity ratio (0.017). The data reflect a short initial transient due to starting the experiment (as explained earlier), followed by a period during which condensate accumulates at an almost steady rate; i.e., dM/dt is constant. This steady accumulation period lasts for roughly 300 s, ending at about $t = 400$ s. However, note that for the higher face velocity of 1.5 m/s, dM/dt is larger than for the low face velocity case of 0.8 m/s. Assuming dM/dt is equal to the condensation rate, which would be true if no drainage occurs during this period, then a larger dM/dt is directly attrib-

utable to a larger convection coefficient. Thus, the increase in face velocity gives rise to an increased convection coefficient, which in turn increases dM/dt. After some period of a nearly constant dM/dt, the heat exchanger begins to shed condensate, and dM/dt approaches zero—the point at which shedding equals the condensation rate. In some operating conditions, as shown in the Fig. 15, $M(t)$ can overshoot its final value. From our experiments, the existence of an overshoot depends on the face velocity, with an overshoot occurring at a high face velocity.

A possible explanation of how face velocity is related to this overshoot behavior can be formulated by recognizing there are several drainage paths for condensate on the heat exchanger: it can drain through the louvers and down the fin; it can drain along the tube surfaces, or it can flow to the exit face and drain. At low velocities, the airflow forces are insufficient to push condensate to the exit face, and all drainage is down the fins and tubes. However, when the velocity is high, shear and pressure can cause condensate to flow to the exit face and drain. Before $t = 400$ s, condensate accumulates on the fin and tubes, and due to the blockage effect, the flow eventually pushes it to the exit plane, where it rapidly drains and causes the sudden drop in condensate mass. This behavior does not occur at low velocity, because the deposition rates are lower and the shear and pressure drop are not large enough to cause the condensate to move to the exit plane before it drains down the fins and tubes. Once the drainage paths are established, constant retention is achieved. Further validation would require careful measurement of local drainage. There might be other explanations, such as a redistribution of condensate droplet and bridge sizes cause by the air flow.

In addition to the important effect of face velocity on the real-time condensate accumulation, it is important to the steady-state retention of condensate as shown in Fig. 16. For the five coils shown in Fig. 16, less condensate is retained at higher velocities, as expected. For example, a louver fin (coil 2) shows a 50% reduction in retention as the face velocity increases from 1 m/s to 2 m/s. A combination fin (coil 4) decreased only 25% for the same velocity change. The effect of velocity appears to be most closely related to geometry rather than surface condition, and this relationship is suggested by noting that no great differences in advancing and receding contact angle for these five coils. We note the above experiments were conducted over a limited range, with a limited set of heat exchangers, thus, more work is needed to support the generality of our conclusion.

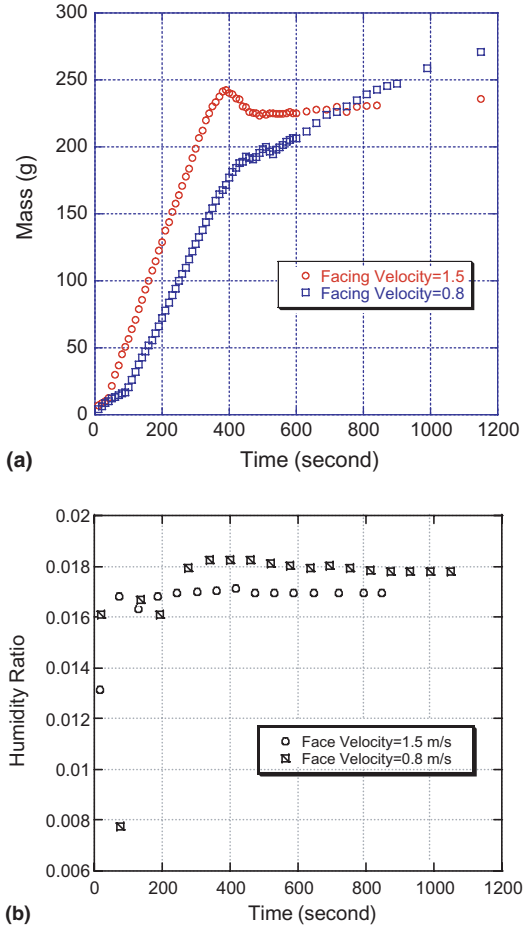

Fig. 15. Real-time condensate retention data for coil 4 at two air-side face velocities in wind-tunnel experiments: (a) shows an overshoot in retention at the higher velocity but a monotonic increase in condensate loading at the lower face velocity; (b) because the humidity ratio in these transient experiments is difficult to control, the humidity ratio as a function of time for the experiments of (a) are presented.

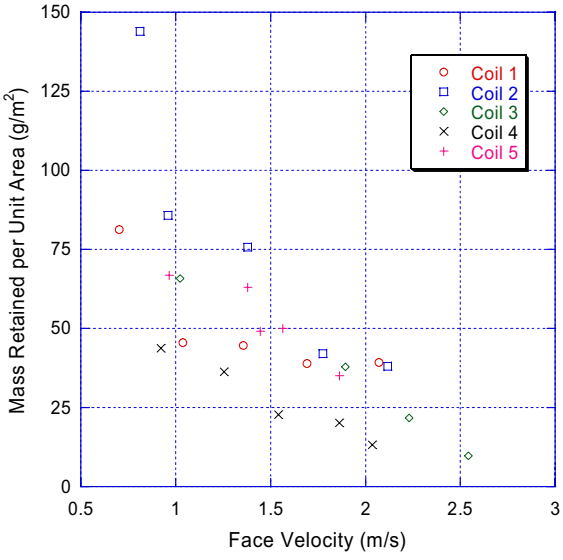

Fig. 16. Steady-state condensate retention per unit of heat transfer area as a function of face velocity from wind-tunnel experiments for five coils. The data clearly show that condensate retention, for a range of coils, depends on the face velocity.

5. Conclusions

An important finding of this research follows from comparing the dip-test and steady-state retention results. Among the coils (coils 2 through 5) tested both in dip testing and in wind-tunnel testing, the coil retaining the most condensate in the steady-state wind-tunnel tests holds the most water in the dip test (coil 2); the coil holding the least condensate in steady-state testing holds the least in dip testing (coil 4). Although the two methods have completely different experimental bases, it appears dynamic dip testing can be a powerful tool for assessing the condensate retention behavior of a coil. Dynamic dip testing is fast, simple, cheap and repeatable, and might show some information about drainage patterns, off-cycle retention, and forces on the condensing surface.

There are several other interesting findings from dynamic dip testing. First, results from dip testing show different drainage patterns, some heat exchangers drain water continuously while the others reach a steady state quickly (Fig. 7). For the specimens tested shown in Fig. 7, the offset strip fin (coils 6 and 7) holds the least water and the louver fin (coils 2 and 3) the most water. This finding motivated the development of the so-called combination fin (coils 4 and 5), with the hope of exploiting the thermal–hydraulic performance of the louver fin and the condensate management behavior of the offset strip fin. Second, the drainage data reported in this paper show profound differences in the round-tube and the flat-tube drainage behavior, with very rapid drainage from the round-tube geometry, and a slower process for flat-tube heat exchangers (shown in Fig. 8). Third, we hypothesize the drainage path to be through the inter-fin space of the round-tube heat exchanger, and through the inter-louver gap for the flat-tube heat exchanger, our model is highly successful in predicting the magnitude and trends of the data as shown in Fig. 9, supporting the assumed drainage paths. Moreover, using the model, it is possible to ascertain the relative importance of drainage forces. Gravity dominates drainage in the round-tube geometry, but viscous effects become important in the flat-tube heat exchanger as shown in Fig. 10. Fourth, another impact on retention is the fin geometry and the construction of the coil at the bottom. In general, coils with two manifolds performed better than coils with only one manifold at its top. Coils with rectangular fins (viewed from the air flow direction) hold less water than coils with triangular fins. Finally, in the range of the current experiments, inclination of the coils has very little effect on drainage pattern; it reduces a little amount of water retention at a given time, especially for less compact (larger fin pitch) heat exchangers.

Another contribution of this work rests in the real-time retention data, which show the possibility of overshoot in condensate retention. Heat exchanger designers should avoid geometry and operating conditions that give rise to such an overshoot, because the sudden discharge of condensate from the coil might result in blow-off into the passenger compartment.

Acknowledgments

This work was financially supported by the Air-Conditioning and Refrigeration Technology Institute (ARTI) under 21-CR, Elizabeth Jones program director, and by Visteon Climate Control Systems Ltd, Dr. Chao Zhang program director. Their support is gratefully acknowledged.

References

[1] D.L. Katz, J.M. Geist, Condensation of six finned tubes in a vertical row, ASME Transactions (Nov) (1948) 908–914.
[2] V.A. Karkhu, V.P. Borovkov, Film condensation of vapor at finely-finned horizontal tubes, Heat Transfer—Soviet Research 3 (2) (1971) 183–191.
[3] V.G. Rifert, P.A. Barabash, A.B. Golubev, G.G. Leot'yev, S.I. Chaplinskey, Investigation of film condensation enhanced by surface forces, Heat Transfer—Soviet Research 9 (2) (1977) 23–27.
[4] H. Honda, S. Nozu, K. Mitsumori, Augmentation of condensation on horizontal finned tubes by attaching a porous drainage plate, in: Proceedings of ASME-JSME Joint Thermal Engineering Conference, Honolulu, Hawaii, March 1983, pp. 20–24.
[5] T.M. Rudy, R.L. Webb, An Analytical model to predict condensate retention on horizontal integral-fin tubes, Journal of Heat Transfer 107 (1985) 361–368.
[6] H. Osada, H. Aoki, T. Ohara, I. Kuroyanagi, Experimental analysis for enhancing automotive evaporator fin performance, in: R.K. Shah (Ed.), Proceedings of the International Conference on Compact Heat Exchangers and Enhancement Technology for the Process Industries, 1999, pp. 439–445.
[7] H. Osada, H. Aoki, T. Ohara, I. kuroyanagi, Research on corrugated multi-louvered fins under dehumidification, Heat Transfer—Asian Research 30 (2001) 383–393.
[8] W.J. McLaughlin, R.L. Webb, Condensate drainage and retention in louver fin automotive evaporators, in: Proceedings of the SAE International Congress, Detroit, MI, March 2000, No. 2000-01-0575.
[9] W.J. McLaughlin, The effect of condensate on the air side performance of louver fin automotive evaporators, MS thesis, Department of Mechanical Engineering, Pennsylvania State University, 1999.
[10] C. Korte, A.M. Jacobi, Condensate retention effects on the performance of plain-fin-and-tube heat exchangers: Retention data and modeling, Journal of Heat Transfer 123 (5) (2001) 926–936.
[11] B.R. Bull, A.M. Jacobi, A study of the application of vortex generators to enhance the air-side performance of heat exchangers, Technical Report TR-214, Air Conditioning and Refrigeration Center, University of Illinois at Urbana-Champaign, 2003.
[12] G.J. Kim, A.M. Jacobi, Condensate accumulation effects on the air-side thermal performance of slit-fin surfaces, Contract Report CR-26, Air Conditioning and Refrigeration Center, University of Illinois at Urbana-Champaign, 2000.
[13] ASHRAE, ASHRAE Handbook—Fundamentals, American Society of Heating, Refrigerating and Air-Conditioning Engineers, Inc., Atlanta, GA, 2001.